Higgs Pair Production at the LHC through the Flavon

Marco A. Arroyo-Ureña,[1,2,*] Amit Chakraborty,[3,†] J. Lorenzo Díaz-Cruz,[1,4,‡] Dilip Kumar Ghosh,[5,§] Najimuddin Khan,[6,¶] and Stefano Moretti[7,8,**]

[1] *Centro Interdisciplinario de Investigación y Enseñanza de la Ciencia (CIIEC), Benemérita Universidad Autónoma de Puebla, C.P. 72570, Puebla, México*

[2] *Departamento de Física, FES Cuautitlán, Universidad Nacional Autónoma de México, Estado de México, 54770, México*

[3] *Department of Physics, School of Engineering and Sciences, SRM University AP, Amaravati, Mangalagiri 522240, India*

[4] *Facultad de Ciencias Fisico-Matematicas, BUAP. Apdo. Postal 1364, C.P. 72000 Puebla, México*

[5] *School of Physical Sciences, Indian Association for the Cultivation of Science, 2A & 2B Raja S.C. Mullick Road, Kolkata 700032, India*

[6] *Harish-Chandra Research Institute, A CI of Homi Bhabha National Institute, Chhatnag Road, Jhunsi, Prayagraj 211019, India*

[7] *School of Physics & Astronomy, University of Southampton, Highfield, Southampton SO17 1BJ, UK*

[8] *Department of Physics & Astronomy, Uppsala University, Box 516, SE-751 20 Uppsala, Sweden*

Abstract

The detection of a single Higgs boson at the Large Hadron Collider (LHC) has allowed one to probe some properties of it, including the Yukawa and gauge couplings. However, in order to probe the Higgs potential, one has to rely on new production mechanisms, such as Higgs pair production. In this paper, we show that such a channel is also sensitive to the production and decay of a so-called 'Flavon' field (H_F), a new scalar state that arises in models that attempt to explain the hierarchy of the Standard Model (SM) fermion masses. In particular, we show that, with 300 fb^{-1} of accumulated data at 14 TeV (the Run 3 stage) of the LHC an heavy Flavon H_F with mass $M_{H_F} \simeq 2m_t$ can be explored with 5σ significance through the channel $pp \to H_F \to hh$ ($h \to \gamma\gamma, h \to b\bar{b}$). However, to probe the $M_{H_F} \sim 1$ TeV range, one has to rely on the High-Luminosity LHC (HL-LHC).

*Electronic address: marroyo@comunidad.unam.mx
†Electronic address: amit.c@srmap.edu.in
‡Electronic address: jldiaz@fcfm.buap.mx
§Electronic address: tpdkg@iacs.res.in
¶Electronic address: najimuddinkhan@hri.res.in
**Electronic address: s.moretti@soton.ac.uk; stefano.moretti@physics.uu.se

I. INTRODUCTION

The discovery of a Higgs boson [1–3] with mass $M_h = 125.5$ GeV has provided a firm evidence for the mechanism of Electro-Weak Symmetry Breaking (EWSB) based on a Higgs potential [4, 5] pointing towards the minimal realization of it that defines the Standard Model (SM). So far, the corresponding studies have relied on the four standard single Higgs production mechanism, i.e., gluon-gluon fusion, vector boson fusion, Higgs-strahlung and associated production with top-quark pairs (see Ref. [6]), which have permitted to extract the Higgs boson couplings with quarks (b and t), leptons (τ and μ) and gauge bosons (W and Z) as well as the effective interaction with photon and gluon pairs. However, there still remains the task of probing the Higgs self-coupling. Higgs boson pair (hh) production provides a direct probe of the Higgs boson self-coupling, which directly controls the size of the hh production cross section. In fact, in the SM, the non-resonant pair production of Higgs bosons is the only direct probe to measure the Higgs boson self-coupling. However, the smallness of the cross section makes it difficult to measure the coupling with a good precision. Next-to-Leading Order (NLO) effects help somewhat to improve the situation [7–9].

Di-Higgs production is significantly enhanced in many new physics models. Studies have shown that, for example, scenarios with an extended Higgs sector, new heavy resonances, Supersymmetric theories, Effective Field Theories (EFTs) with modified top Yukawa coupling, etc., di-Higgs production receives additional contributions along with the SM ones [10–42]. These effects make the study of the di-Higgs production process interesting and, at the same time, also very challenging. In particular, the possibility to produce Higgs pairs in the decay of a new heavy particle that belongs to the spectrum of those models offers some hope to achieve detectable signals at current and future colliders. Specifically, we will study the interactions of the discovered Higgs boson with the so-called 'Flavon' field H_F that appears in models that attempt to explain the hierarchy of quark and lepton masses using the Froggatt-Nielsen (FN) mechanism [43]. This mechanism assumes that, above some scale M_F roughly corresponding to the Flavon mass, there is a symmetry, perhaps of Abelian type $U(1)_F$, with the SM fermions being charged under it, which then forbids the appearance of Yukawa couplings at the renormalizable level. However, Yukawa matrices can arise through non-renormalizable operators. The Higgs spectrum of these models includes a light H_F state, which could mix effectively with the SM Higgs boson when the flavor scale is of the order 1 TeV or lower. Recently, the phenomenology of Higgs vs Flavon interactions at particle colliders has been the focus of some attention [44–50]. In particular, within this framework, it is possible to have a coupling of this new scalar with Higgs boson pairs, which can then provide interesting signals to be searched for at the LHC, indeed, in the discussed (SM-like) Higgs pair production.

In this paper, we are interested in studying the detection of the Flavon signal emerging from the production and decay process $pp \to H_F \to hh$ ($h \to \gamma\gamma, h \to b\bar{b}$) at future stages of the LHC, namely, Run 3 and the High-Luminosity LHC (HL-LHC) [51, 52]. We ignore considering here the $pp \to H_F \to hh$ ($h \to \tau^+\tau^-, h \to b\bar{b}$) channel, which could indeed be competitive with our chosen signal, so we leave it for a future publication.

The ATLAS and CMS collaborations at the LHC have already performed several studies of non-resonant di-Higgs production with various possible final states using both Run 1 and the Run 2 dataset. None of these searches have observed a statistically significant excess over the SM background, therefore, upper limits on the di-Higgs production cross section are placed [53–62].

We focus here on the '2 photons plus 2 b-jets' final state. This particular (comparatively clean) final state obtained through $pp \to H_F \to hh$ production followed by $h \to \gamma\gamma$ and $h \to b\bar{b}$ decays has large significances in specific parameter space regions in the context of the LHC operated at $\sqrt{s} = 14$ TeV of energy with integrated luminosities of both 300 and 3000 fb^{-1}. Besides these future energies and luminosities, we also present our result based on the data set accumulated to date, i.e., with a luminosity of 139 fb^{-1} at the 13 TeV LHC (Run 2). The advocated signature of the SM di-Higgs process has been explored earlier in the literature, albeit in different scenarios [10–42], while the analysis of $pp \to H_F \to hh$ ($h \to \gamma\gamma, h \to b\bar{b}$) in the context of the present model has not been discussed in any depth [44–49]. Our analysis of this final state gives promising results as a discovery channel for a heavy CP-even H_F boson in the aforementioned FN framework. In order to prove this, we first choose three sets of reference points for three heavy Higgs masses, 300, 600 and 900 GeV. A signal region (a set of different kinematic cuts) is then defined to maximize signal significances in the presence the SM backgrounds having the same final state. In our cut-based analysis, we further use the same signal region for different combinations of the singlet scalar Vacuum Expectation Value (VEV) v_s and heavy Higgs mass M_{H_F} to compute the signal significances. The latter are only mildly affected (at the $5-10\%$ level) by incorporating a realistic 5% systematic uncertainty in the SM background estimation. We find a large number of signal events that have significances exceeding 5σ and they can be explored with both 300 fb^{-1} and 3000 fb^{-1} of data at LHC runs using $\sqrt{s} = 14$ TeV. We also extract the current observed limit at 95% CL (Confidence Level) from direct heavy Higgs (or Flavon) searches in the '2 photons plus 2 b-jets' final state derived by ATLAS using the LHC dataset collected at $\sqrt{s} = 13$ TeV with a luminosity of $\mathcal{L} = 139$ fb^{-1}.

The rest of the paper is organized as follows. In sec. II, we present the details of the model and derive expressions for the masses and relevant interaction couplings for all the particles. Afterwards, we introduce the constraints acting on it from both the theoretical and experimental side (in sec. III). The possible collider signals arising from the decay of the Flavon are then analyzed. Finally, we conclude in sec. V.

II. THE MODEL

We now focus on some relevant theoretical aspects of what we will refer to as the FN singlet Model (FNSM). In Ref. [63], a comprehensive theoretical analysis of the Higgs potential therein is presented along with the constraints on the parameter space from the Higgs boson signal strengths and the oblique parameters, including presenting a few benchmark scenarios amenable to phenomenological investigation. (See Ref. [64] for the effects of Lepton Flavor Violation (LFV).)

A. The scalar sector

The scalar sector of this model consists of the SM Higgs doublet Φ ane and one SM singlet complex FN scalar S_F. In the unitary gauge, we parameterize these fields as:

$$\Phi = \begin{pmatrix} 0 \\ \frac{v+\phi^0}{\sqrt{2}} \end{pmatrix}, \tag{2.1}$$

$$S_F = \frac{(v_s+S_R+iS_I)}{\sqrt{2}}, \tag{2.2}$$

where v and v_s represent the VEVs of the SM Higgs doublet and FN singlet, respectively. The scalar potential should be invariant under the FN $U(1)_F$ flavor symmetry. Under this symmetry, the SM Higgs doublet H and FN singlet S_F transform as $\Phi \to \Phi$ and $S_F \to e^{i\theta} S_F$, respectively.

In general, such a scalar potential admits a complex VEV, $\langle S_F \rangle_0 = \frac{v_s}{\sqrt{2}} e^{i\xi}$, but in this work we consider the special case in which the Higgs potential is CP-conserving, by setting the phase $\xi = 0$. Such a CP-conserving Higgs potential is then given by:

$$V_0 = -\frac{1}{2} m_1^2 \Phi^\dagger \Phi - \frac{1}{2} m_2^2 S_F^* S_F + \frac{1}{2} \lambda_1 \left(\Phi^\dagger \Phi\right)^2 + \lambda_2 \left(S_F^* S_F\right)^2 + \lambda_3 \left(\Phi^\dagger \Phi\right) \left(S_F^* S_F\right). \tag{2.3}$$

The $U(1)_F$ flavor symmetry of this scalar potential is spontaneously broken by the VEVs of the spin-0 fields (Φ, S_F) and this leads to a massless Goldstone boson in the physical spectrum. In order to give a mass to it, we add the following soft $U(1)_F$ breaking term to the potential:

$$V_{\text{soft}} = -\frac{m_3^2}{2} \left(S_F^2 + S_F^{*2}\right). \tag{2.4}$$

The full scalar potential is thus:

$$V = V_0 + V_{\text{soft}}. \tag{2.5}$$

The presence of the λ_3 term allows mixing between the Flavon and the Higgs fields after both the $U(1)_F$ flavor and EW symmetry breaking and contributes to the mass parameters for both the Flavon and Higgs field, as can be seen below. The soft $U(1)_F$ flavor symmetry breaking term V_{soft} is responsible for the pseudoscalar Flavon (S_I) mass. Once the minimization conditions for the potential V are applied, we obtain the following relations between the parameters of V:

$$m_1^2 = v^2 \lambda_1 + v_s^2 \lambda_3, \tag{2.6}$$

$$m_2^2 = -2m_3^2 + 2v_s^2 \lambda_2 + v^2 \lambda_3. \tag{2.7}$$

All the parameters of the scalar potential are real and therefore the real and imaginary parts of

V do not mix. The CP-even mass matrix can be written in the (ϕ_0, S_R) basis as:

$$M_S^2 = \begin{pmatrix} \lambda_1 v^2 & \lambda_3 v v_s \\ \lambda_3 v v_s & 2\lambda_2 v_s^2 \end{pmatrix}. \tag{2.8}$$

The corresponding mass eigenstates are obtained via the standard 2×2 rotation:

$$\phi^0 = \cos\ \alpha\ h + \sin\ \alpha\ H_F, \tag{2.9}$$

$$S_R = -\sin\ \alpha\ h + \cos\ \alpha\ H_F, \tag{2.10}$$

with α a mixing angle. Here h is identified with the SM-like Higgs boson with mass M_h=125.5 GeV whereas the mass eigenstate H_F is the CP-even Flavon. The corresponding CP-odd Flavon $A_F \equiv S_I$ will have a mass such that $M_{A_F}^2 = 2m_3^2$. Both H_F and A_F are considered to be heavier than h. In this model, we will work with the mixing angle α and physical masses M_h, M_{H_F} and M_{A_F}, which are related to the quartic couplings of the scalar potential in Eq. (2.3) as follows:

$$\begin{aligned} \lambda_1 &= \frac{\cos\alpha^2 M_h^2 + \sin\alpha^2 M_{H_F}^2}{v^2}, \\ \lambda_2 &= \frac{M_{A_F}^2 + \cos\alpha^2 M_{H_F}^2 + \sin\alpha^2 M_h^2}{2v_s^2}, \\ \lambda_3 &= \frac{\cos\alpha\ \sin\alpha}{v v_s}\,(M_{H_F}^2 - M_h^2). \end{aligned} \tag{2.11}$$

We consider the mixing angle α, the FN singlet VEV v_s and its (pseudo)scalar field masses M_{H_F,A_F} as free parameters in this work.

B. Yukawa sector

The effective $U(1)_F$ invariant Yukawa Lagrangian, á la FN, is given by [43]:

$$\begin{aligned} \mathcal{L}_Y = &\rho_{ij}^d \left(\frac{S_F}{\Lambda_F}\right)^{q_{ij}^d} \bar{Q}_i d_j \tilde{\Phi} + \rho_{ij}^u \left(\frac{S_F}{\Lambda_F}\right)^{q_{ij}^u} \bar{Q}_i u_j \Phi \\ &+ \rho_{ij}^\ell \left(\frac{S_F}{\Lambda_F}\right)^{q_{ij}^l} \bar{L}_i \ell_j \Phi + \text{h.c.}, \end{aligned} \tag{2.12}$$

where $\rho^{u/d/\ell}$ are dimensionless couplings seemingly of order one. This will lead to Yukawa couplings once the $U(1)_F$ flavor symmetry is spontaneously broken. The integers q_{ij}^f ($f = u,\ d,\ \ell$) are the combination of $U(1)_F$ charges of the respective fermions. In order to generate the Yukawa couplings, one spontaneously breaks both the $U(1)_F$ and EW symmetries. In the unitary gauge one can make the following first order expansion of the neutral component of the heavy Flavon

Vertex (ϕXX)	Coupling constant ($g_\phi XX$)
$hf_i\bar{f}_j$	$\frac{c_\alpha}{v}\tilde{M}^f_{ij} - s_\alpha r_s \tilde{Z}^f_{ij}$
$H_F f_i \bar{f}_j$	$\frac{s_\alpha}{v}\tilde{M}^f_{ij} + c_\alpha r_s \tilde{Z}^{f_{ij}}$
$A_F f_i \bar{f}_j$	$i\, r_s \tilde{Z}^{f_{ij}}$
hZZ	$i\,\frac{gM_Z}{c_W} c_\alpha$
hWW	$i\, g M_W c_\alpha$
$H_F ZZ$	$i\,\frac{gM_Z}{c_W} s_\alpha$
$H_F WW$	$i\, g M_W s_\alpha$
$H_F hh$	$-i\{c_\alpha^3\lambda_3 v_s + c_\alpha^2 s_\alpha v(3\lambda_1 - 2\lambda_3) - 2c_\alpha s_\alpha^2 v_s(\lambda_3 - 3\lambda_2) + \lambda_3 s_\alpha^3 v\}$ $\equiv -i\,\{c_\alpha s_\alpha(3M^2_{A_F} s_\alpha v + (M^2_{H_F} + 2M_h^2)(s_\alpha v + c_\alpha v_s))\}/(v v_s)$
$A_F hh$	0

TABLE I: Tree-level couplings of the SM-like Higgs boson h and the Flavons H_F and A_F to fermion and gauge boson pairs in the FNSM. Here, $r_s = v/\sqrt{2}v_s$.

field S_F around its VEV v_s:

$$\left(\frac{S_F}{\Lambda_F}\right)^{q_{ij}} = \left(\frac{v_s + S_R + iS_I}{\sqrt{2}\Lambda_F}\right)^{q_{ij}} \simeq \left(\frac{v_s}{\sqrt{2}\Lambda_F}\right)^{q_{ij}} \left[1 + q_{ij}\left(\frac{S_R + iS_I}{v_s}\right)\right], \tag{2.13}$$

which leads to the following fermion couplings after replacing the mass eigenstates in $\mathcal{L}_Y$:

$$\begin{aligned}\mathcal{L}_Y \;=\; & \frac{1}{v}[\bar{U}M^u U + \bar{D}M^d D + \bar{L}M^\ell L](c_\alpha h + s_\alpha H_F) \\ & +\; \frac{v}{\sqrt{2}v_s}[\bar{U}_i \tilde{Z}^u_{ij} U_j + \bar{D}_i \tilde{Z}^d_{ij} D_j + \bar{L}_i \tilde{Z}^\ell_{ij} L_j] \\ & \times\; (-s_\alpha h + c_\alpha H_F + iA_F) + \text{h.c.},\end{aligned} \tag{2.14}$$

where we define $\sin\alpha \equiv s_\alpha$ and $\cos\alpha \equiv c_\alpha$. Here, M^f stands for the diagonal fermion mass matrix while the intensities of the Higgs-Flavon couplings are encapsulated in the $\tilde{Z}^f_{ij} = U^f_L Z^f_{ij} U^{f\dagger}_L$ matrices. In the flavor basis, the Z^f_{ij} matrix elements are given by:

$$Z^f_{ij} = \rho^f_{ij}\left(\frac{v_s}{\sqrt{2}\Lambda_F}\right)^{q^f_{ij}} q^f_{ij}, \tag{2.15}$$

which remains non-diagonal even after diagonalizing the mass matrices, thereby giving rise to FV scalar couplings. In addition to the Yukawa couplings we also need the ϕVV ($V = W, Z$) couplings for our calculation which can be extracted from the kinetic terms of the Higgs doublet and complex singlet. In Tab. I we show the coupling constants for the interactions of the SM-like Higgs boson and the Flavon to fermions and gauge bosons.

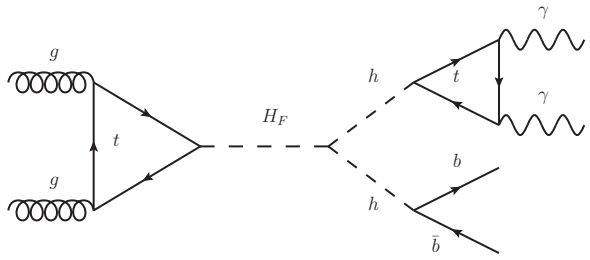

FIG. 1: Representative Feynman diagram of the signal $gg \to H_F \to hh$ $(h \to b\bar{b}, h \to \gamma\gamma)$.

III. CONSTRAINTS ON THE FNSM PARAMETER SPACE

In order to perform a realistic numerical analysis of the signal $pp \to H_F \to hh$ $(h \to b\bar{b}, h \to \gamma\gamma)$ (see Fig. 1), we need to constrain the free parameters, i.e.: (i) the mixing angle α of the real components of the doublet Φ and the FN singlet S, (ii) FN singlet VEV v_s, (iii) the heavy (pseudo)scalar field masses M_{H_F,A_F} and (iv) the diagonal $\tilde{Z}^u_{33} \equiv \tilde{Z}_{tt}$ and $\tilde{Z}^u_{22} \equiv \tilde{Z}_{bb}$ matrix elements which will be used to evaluate both the production cross section of the Flavon H_F and the decay of the Higgs boson to a pair of b quarks; all of which have an impact on the upcoming calculations. These parameters are constrained by various kinds of theoretical bounds like absolute vacuum stability, triviality, perturbativity and unitarity of scattering matrices and different experimental data, chiefly, LHC Higgs boson coupling modifiers, null results for additional Higgs states plus the muon and electron anomalous magnetic (dipole) moments Δa_μ and Δa_e, respectively. The various LFV processes $\tau \to 3\mu$, $\mu \to 3e$, $\tau \to \mu\gamma$, $\mu \to e\gamma$, $B^0_s \to \mu^+\mu^-$ and the total decay width of the Higgs boson (Γ^h_T) are also modified in the presence of these new Yukawa couplings, so they have also been tested against available data. In the following, we discuss the various constraints on the model parameters in turn.

A. Stability of the Scalar Potential

The absolute stability of the scalar potential in Eq. (2.3) requires that the potential should not become unbounded from below, i.e., it should not approach negative infinity along any direction of the field space (h, H_F, A_F) at large field values. Since in this limit the quadratic terms in the scalar potential are negligibly small as compared to the quartic terms, the absolute stability conditions are [65]:

$$\lambda_1(\Lambda) > 0, \quad \lambda_2(\Lambda) > 0 \quad \text{and} \quad \lambda_3(\Lambda) + \sqrt{2\lambda_1(\Lambda)\lambda_2(\Lambda)} > 0, \tag{3.1}$$

wherein these quartic couplings are evaluated at a scale Λ using Renormalization Group Evolution (RGE) equations. If the the scalar potential in Eq. (2.3) has a metastable EW vacuum, then these conditions are modified [65]. One can then use] Eq. (2.11) to translate these limits into those on

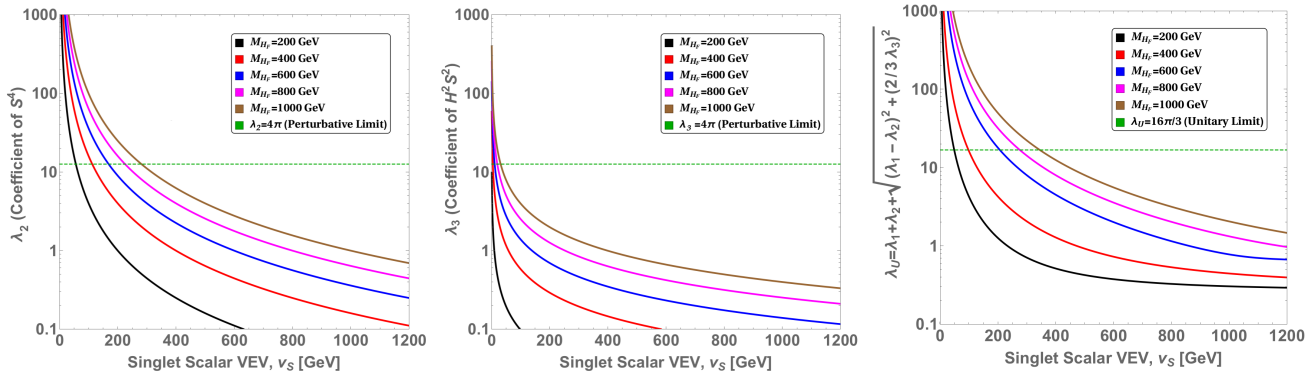

FIG. 2: In the first two plots we show the perturbative bounds on the quartic couplings $\lambda_{2,3}$ while the third plot shows the stringent unitary bounds on λ_U.

the free parameters (as discussed above).

B. Perturbativity and Unitarity Constraints

To ensure that the radiatively improved scalar potential of the FNSM remains perturbative at any given energy scale, one must impose the following upper bounds on the quartic couplings:

$$| \lambda_1(\Lambda), \lambda_2(\Lambda), \lambda_3(\Lambda) | \leq 4\pi. \tag{3.2}$$

The quartic couplings in the scalar potential of our scenario are also severely constrained by the unitarity of the Scattering matrix (S-matrix). At very large field values, one can get the S-matrix by using various (pseudo)scalar-(pseudo)scalar, gauge boson-gauge boson and (pseudo)scalar-gauge boson interactions in $2 \to 2$ body processes. The unitarity of the S-matrix demands that the eigenvalues of it should be less than 8π [65, 66]. In the FNSM, the unitary bounds are obtained from the S-matrix (using the equivalence theorem) as:

$$\lambda_1(\Lambda) \leq 16\pi \quad \text{and} \quad \left|\lambda_1(\Lambda) + \lambda_2(\Lambda) \pm \sqrt{(\lambda_1(\Lambda) - \lambda_2(\Lambda))^2 + (2/3\lambda_3(\Lambda))^2}\right| \leq 16/3\pi. \tag{3.3}$$

We now use the relation in Eq. (2.11) to display theoretical bounds on the scalar singlet VEV v_s for various values of the heavy Higgs masses, M_{H_F} and M_{A_F}. In Fig. 2 we display the constraints on scalar quartic couplings coming from the perturbativity and unitarity of the S-matrix. Here, we assume $M_{H_F} = M_{A_F}$ and $\cos\alpha = 0.995$, which agrees with the constraints from the Higgs boson coupling modifiers from the LHC measurements, which we will discuss in some detail later. Fig. 2(left) shows the $v_s - \lambda_2$ plane for $M_{H_F} = 200$, 400, 600, 800 and 1000 GeV whereas in Fig. 2(middle) the $v_s - \lambda_3$ plane is presented. The plane $v_s - \lambda_U (\equiv \lambda_1 + \lambda_2 + \sqrt{(\lambda_1 - \lambda_2)^2 + (2/3\lambda_3)^2})$ in Fig. 2(right) shows the unitary bounds. We find that $|\lambda_U| \leq 16\pi/3$ is the most stringent upper bound for the scalar quartic couplings. From these plots, we can see

that the lower limit on the scalar singlet VEV v_s is, for $M_{H_F} = (200, 400, 600, 800, 1000)$ GeV, $v_s \geq (69, 138, 207, 276, 345)$ GeV. Note that we are working at the EW scale only, as detailed RGE analysis is beyond the scope of this work. We also choose the parameters in such a way that the scalar potential remains absolutely stable in all the directions of the scalar fields h, H_H, A_F. (Further details can be found in Ref. [65].)

C. Experimental Constraints

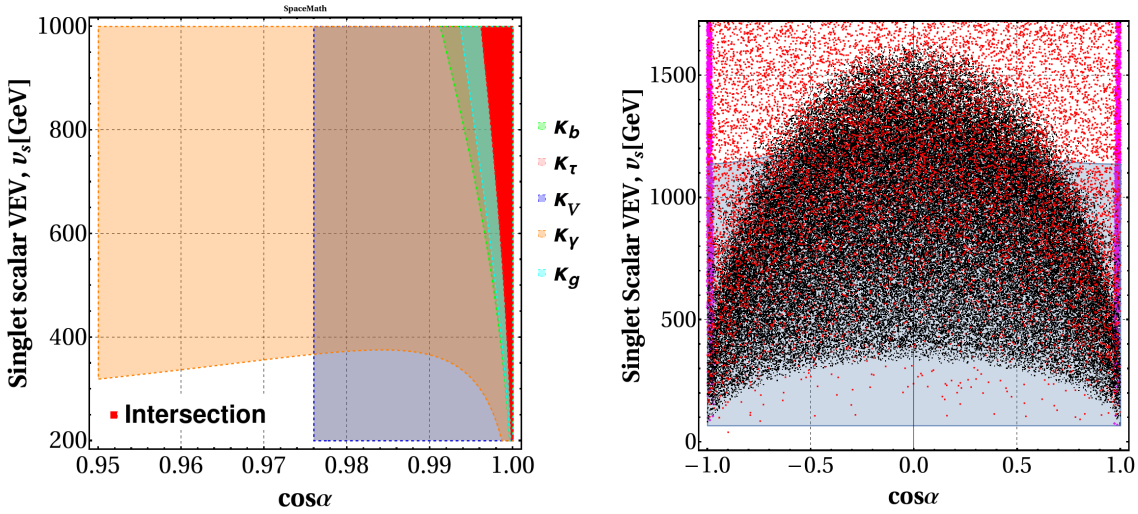

(a) (b)

FIG. 3: VEV of the FN singlet v_s as a function of the cosine of the mixing angle α: constraints are from (a) the SM-like Higgs boson coupling modifiers and (b) flavor observables (as described in the text).

To constrain the mixing angle α and the VEV of the FN singlet v_s, we use HL-LHC projections for the Higgs boson coupling modifiers κ_i at a CL of 2σ [67], as this machine configuration is the one with highest sensitivity among those we will consider in the analysis section. For a production cross section $\sigma(pp \to \phi)$ or a decay width $\phi \to X$ ($\phi = h, h^{\rm SM}$), we introduce:

$$\kappa^2_{pp} = \frac{\sigma(pp \to h)}{\sigma(pp \to h^{\rm SM})}, \quad \kappa^2_X = \frac{\Gamma(h \to X)}{\Gamma(h^{\rm SM} \to X)}, \tag{3.4}$$

where $X = b\bar{b}$, $\tau^-\tau^+$, W^-W^+, ZZ, $\gamma\gamma$. Fig. 3(a) shows all the regions complying with the aforementioned projections for each channel in the $\cos\alpha - v_s$ plane: here, the green, pink, blue, orange and cyan area corresponds to κ_b, κ_τ, κ_V, κ_γ and κ_g, respectively, while the red area represents the intersection of all the areas allowed by all the individual channels. We consider $\tilde{Z}_{bb} = 0.01$ and $\tilde{Z}_{tt} = 0.4$ in the evaluations for the κ_X. Such values are well motivated because they simultaneously accommodate all the κ_X's. In fact, values in the $0.01 \leq \tilde{Z}_{bb} \leq 0.1$ and

$0.1 \leq \tilde{Z}_{tt} \leq 1$ intervals have no important impact on the coupling modifiers, however, in the case when $\tilde{Z}_{bb} \geq 0.1$ and $\tilde{Z}_{tt} \geq 2$, a large reduction of allowed values in the $\cos\alpha - v_s$ plane is found[49, 50].

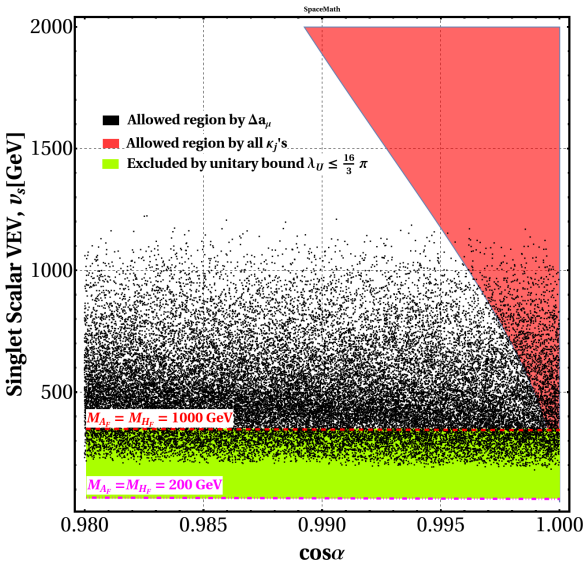

FIG. 4: VEV of the FN singlet v_s as a function of cosine of the mixing angle α in the presence of the most stringent ones among all theoretical and experimental constraints considered.

Furthermore, we present in Fig. 3(b) the $\cos\alpha - v_s$ plane regions allowed by Δa_μ (black points), Δa_e (magenta points), $\mu \to 3e$ (red points) and $B_s^0 \to \mu^+\mu^-$ (blue area). We have also analyzed the decays $\tau \to 3\mu$, $\tau \to \mu\gamma$, $\mu \to e\gamma$, however, these processes are not very restrictive in the FNSM. This is mainly due to the choice we made for the matrix elements $\tilde{Z}_{\mu\mu}$ and $\tilde{Z}_{\tau\tau}$, as they play a subtle role in the couplings (see Tab. I) $\phi\mu^-\mu^+$ and $\phi\tau^-\tau^+$ ($\phi = h$, H_F, A_F), which have a significant impact on the observables $\tau \to 3\mu$, $\tau \to \mu\gamma$, $\mu \to e\gamma$. In fact, we use $\tilde{Z}_{\tau\tau} = 0.2$ and $\tilde{Z}_{\mu\mu} = 10^{-4}$ (hence, a strong hierarchy), otherwise the SM $h\mu^-\mu^+$ coupling would be swamped by new corrections due to the FNSM[1]. So the bounds coming from the processes $\tau \to 3\mu$, $\tau \to \mu\gamma$, $\mu \to e\gamma$ are not included in Fig. 3(b).

Then, in Fig. 4, we display the result of applying all discussed theoretical and experimental constraints, limitedly to the reduced interval $0.98 \leq \cos\alpha \leq 1$, since it is the region in which all the analyzed observables converge. Here, we only show the most restrictive bounds so as to not overload the plot. Among the latter, the unitarity bound plays a special role, as it helped us to find a lower limit for the singlet scalar VEV, v_s, depending on the Flavon mass, e.g., for $M_{H_F} = 1000$ GeV one has $v_s \geq 345$ GeV. By comparison, the intersection of all κ_i's and Δa_μ imposes a less stringent upper limit of $v_s \leq 1200$ GeV[2].

[1] Such a choice was adopted in the evaluation of $\kappa_{\tau\tau}$ and $\kappa_{\mu\mu}$, respectively, and then we scanned on the $\cos\alpha - v_s$ plane, as shown in Fig. 3(a).

[2] Notice that, to generate Figs. 3(a), 3(b) and 4, we have used our own `Mathematica` package, so-called `SpaceMath`

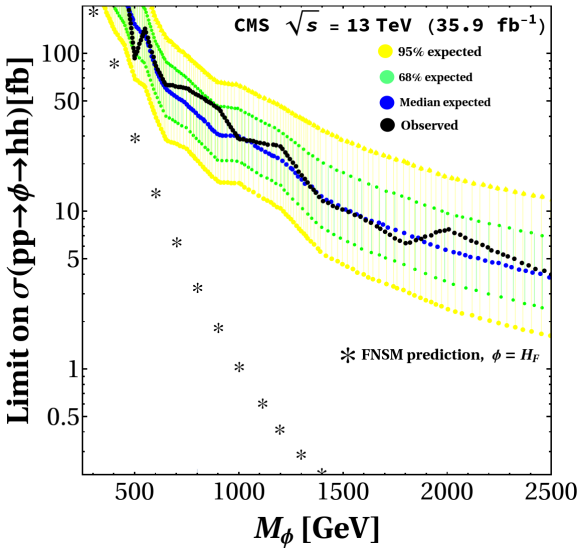

FIG. 5: Expected (blue points) and observed (black points) 95% CL exclusion limits on the production of a narrow, spin-0 resonance (ϕ) decaying into a pair of SM-like Higgs bosons at the LHC. The inner (green fill) and outer (yellow fill) bands indicate the regions containing 68 and 95% CL, respectively, results on the limit applicable to the $pp \to \phi \to hh$ cross section expected under the background-only hypothesis. The starred points are predictions in the FNSM for a selection of heavy Higgs masses ($\phi \equiv H_F$) containing BPs used in our analysis.

Finally, as far as the CP-even Flavon mass M_{H_F} is concerned, to constrain it, we use the limit on the cross section of the process $pp \to \phi \to hh$ from [61], in which a combination of searches for SM-like Higgs boson pair production in proton-proton collisions at $\sqrt{s}$ =13 TeV and 35.9 fb^{-1} is reported. We present in Fig. 5 the cross section of the process $\sigma(pp \to H_F \to hh)$ in the FNSM as a function of M_{H_F} and its comparison with the limit on $\sigma(pp \to \Phi \to hh)$, where ϕ stands for a generic spin-0 resonance. Furthermore, we show in Figs. 6(a) and 6(b) a comparison between the FNSM predictions and the ATLAS Collaboration limits [69], now for individual channels with final states $b\bar{b}b\bar{b}$ and $b\bar{b}\tau^-\tau^+$, respectively. In obtaining such limits, we have evaluated the inclusive cross section of our signal process, wherein we have used $v_s = 1000$ GeV ans $\cos\alpha = 0.995$. It is observed that the $M_{H_F} = 300 - 1000$ GeV interval satisfies the bounds imposed, so we will define Benchmark Points (BPs) with H_F masses herein. The model parameter space in this analysis is also consistent from the other search channels $pp \to H_F \to ZZ$ at ATLAS [70] and $pp \to H_F \to WW$ at CMS [71].

[68], which is available upon request.

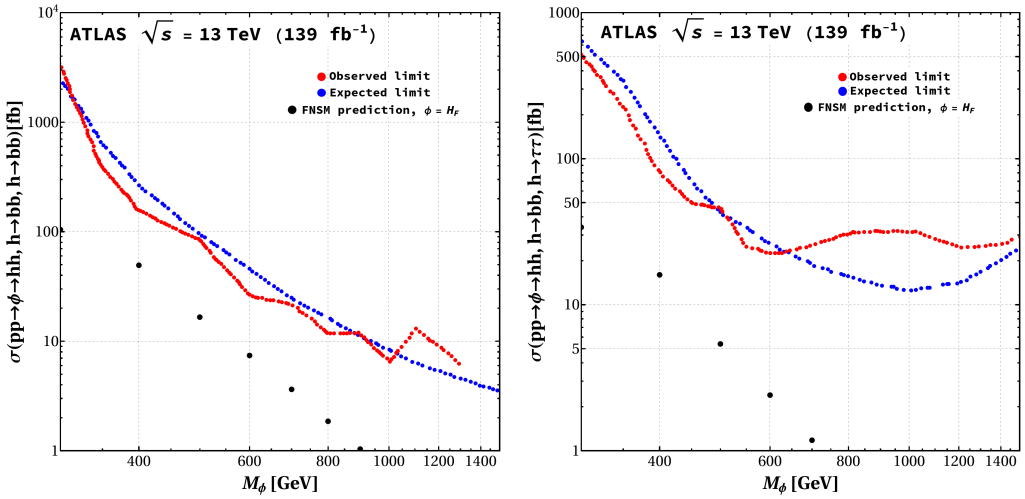

(a) (b)

FIG. 6: Upper limits (observed and expected) on the cross section for di-Higgs production through an intermediate heavy particle ϕ as a function of the particle mass M_ϕ as obtained through the processes $pp \to H_F \to hh$ $(h, \to b\bar{b}, h \to b\bar{b})$ (left) and $pp \to H_F \to hh$ $(h, \to b\bar{b}$, $h \to \tau^+\tau^-)$ (right).

IV. COLLIDER ANALYSIS

Following our discussions on various model parameters and their constraints, we now study the collider signature emerging in the FNSM in the form of a singlet-like CP-even heavy Higgs scalar H_F decaying into SM-like Higgs pairs at Run 3 of the LHC as well as the HL-LHC, assuming $\sqrt{s} = 14$ TeV for both and a luminosity of 300 and 3000 fb^{-1}, respectively. In our analysis, we adopt $c_\alpha = 0.995$ (i.e., a small mixing angle α between the CP-even part of the doublet and singlet scalar fields) and assume for the cut-off scale $\Lambda_F = 10$ TeV, in order to easily avoid theoretical as well as experimental bounds (as discussed in the previous section). Specifically, at the LHC, we consider the resonant production of the H_F state via gluon-gluon fusion, followed by its decay into two on-shell SM-like Higgs bosons (h), wherein one decays into a pair of b-tagged jets while the other decays into two photons, i.e., $pp \to H_F \to hh$ $(h \to b\bar{b},\ h \to \gamma\gamma)$: recall Fig.1. Hence, in the final state, events have two photons (γ) and two b-jets, with some amount of hadronic activity generated from the initial state. Here, we only analyze the channel $H_F \to hh$, since it is to be noted that the $A_F hh$ coupling is zero because of CP conservation, hence the twin production process $pp \to A_F \to hh$ via gluon-gluon fusion is not possible.

We use `FeynRules` [72] to built the FNSM model and produce the UFO files for `MadGraph-2.6.5` [73]. Using the ensuing particle spectrum into `MadGraph-2.6.5`, we calculate the production cross section of the aforementioned production and decay process. The MadGraph_aMC@NLO [73] framework has been used to generate the background events in the SM. Subsequent showering and hadronization have been performed with `Pythia-8` [74]. The de-

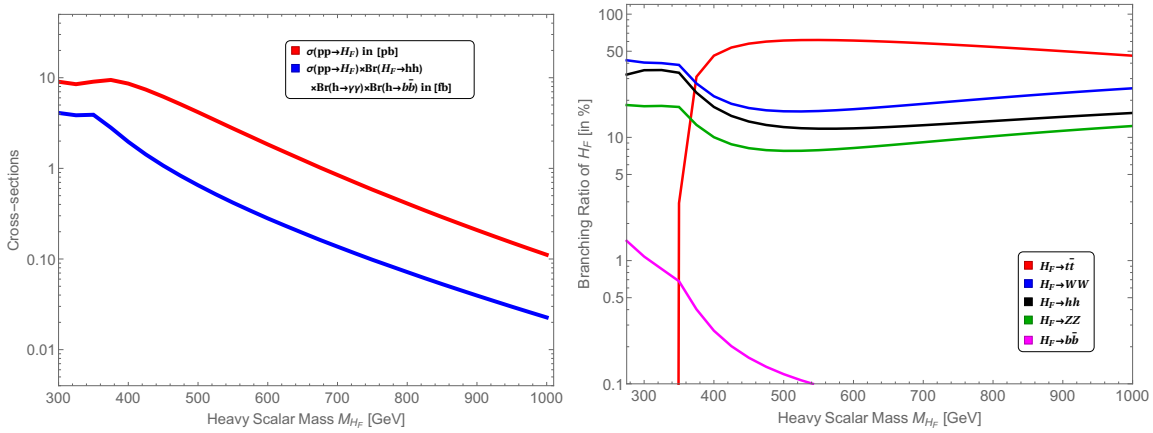

FIG. 7: The red (blue) line on the left plot stands for the cross section of the process $pp \to H_F$ ($pp \to H_F \to hh$ ($h \to \gamma\gamma, h \to b\bar{b}$)) at 14 TeV. The variation in the BRs of the heavy CP-even Flavon mass M_{H_F} is displayed in the right plot.

tector response has been emulated using `Delphes-3.4.2` [75]. The default ATLAS configuration card which comes along with the `Delphes-3.4.2` package has been used in the entirety of this analysis. For both the signal and background processes, we consider the Leading Order (LO) cross sections computed by MadGraph_aMC@NLO, unless stated otherwise.

We first generate the signal events for various heavy CP-even Flavon masses, $M_{H_F}(= M_{A_F})$. The latter have been varied from 260 to 1000 GeV with a step size of 10 GeV. We then take $v_s = 1000$ GeV: such a large VEV produces a small production cross section $\sigma(pp \to H_F)$ and a correspondingly small partial width $\Gamma(H_F \to hh)$, hence small (but non-negligible, for our purposes) signal rates, however, this is necessary to comply with all theoretical and experimental limits. We display the cross section of the process $pp \to H_F$ and $pp \to H_F \to hh$ ($h \to \gamma\gamma, h \to b\bar{b}$) on the left-hand-side of Fig. 7, where the red line stands for $\sigma(pp \to H_F)$.

One can thus understand the nature of the production and decay rates as follows. The production cross sections of the heavy CP-even Flavon H_F (or pseudo scalar A_F, for that matter) mainly depends on the $g_{H_F t\bar{t}} = \frac{c_\alpha v + s_\alpha v_s}{v_s} \frac{y_t}{\sqrt{2}}$ ($g_{A_F t\bar{t}} = \frac{v}{v_s} \frac{y_t}{\sqrt{2}}$) coupling, as the latter goes into the effective Higgs-to-two gluon vertex, hgg. The corresponding term in the Lagrangian is given by [76]:

$$\mathcal{L}_{\rm eff} = \frac{1}{v} g_{hgg}\, h\, G_{\mu\nu} G^{\mu\nu}, \tag{4.1}$$

$$g_{hgg} = -i \frac{\alpha_S}{8\pi} \tau (1 + (1-\tau) f(\tau)) \qquad \text{with} \quad \tau = \frac{4M_t^2}{M_h^2}, \tag{4.2}$$

$$f(\tau) = \begin{cases} (\sin^{-1}\sqrt{\frac{1}{\tau}})^2, & \tau \geq 1, \\ -\frac{1}{4}[\ln \frac{1+\sqrt{1-\tau}}{1-\sqrt{1-\tau}} - i\pi]^2 & \tau < 1. \end{cases} \tag{4.3}$$

In this model, the ggh, ggH_F and ggA_F couplings take the following form: $g_{hgg} = \left(\frac{c_\alpha v_s - s_\alpha v}{v_s}\right) g_{hgg}$,

$g_{H_F gg} = \left(\frac{c_\alpha v + s_\alpha v_s}{v_s}\right) g_{hgg}$ and $g_{A_F gg} = \frac{v}{v_s} g_{hgg}$, respectively. It is to be noted that, for $M_{H_F,A_F} > 2\,M_t$, $f(\tau) = -\frac{1}{4}[\ln\frac{1+\sqrt{1-\tau}}{1-\sqrt{1-\tau}} - i\pi]^2$. Hence, one can understand the shape of the plot by exploiting these functions. The Branching Ratios (BRs) of H_F into various channels for $v_s = 1000$ GeV are shown on the right-hand-side of Fig. 7. From the BR plot, we can see that, for heavier H_F masses, this state dominantly decays into $t\bar{t}$. For small masses, $H_F \to WW$ dominates. Yet, $H_F \to hh$ is always the third largest decay channel.

The major SM backgrounds typically have the form $hh + X$ (where X is known SM particles), which includes SM Higgs pair hh production, $h + X$ like $hZ, hb\bar{b}$ and $ht\bar{t}$, as well as the non-Higgs processes which include $t\bar{t}$ and $t\bar{t}\gamma$ (here, leptons may fake as photons) as well as $b\bar{b}\gamma\gamma$, $c\bar{c}\gamma\gamma$ and $jj\gamma\gamma$ (where c-jets and light-jets may fake b-jets). The other relevant reducible backgrounds comprise $b\bar{b}j\gamma, c\bar{c}j\gamma$ and $b\bar{b}jj$, where c-jets may appear as b-jets and a light-jet may fake a photon. The fake rate of a light-jet j into a photon depends on the momentum of the jet, p_T^j [77], as $9.3 \times 10^{-3}\exp(-p_T^j/27.5\text{ GeV})$. The c-jet is misidentified as a b-jet with a rate of 3.5% whereas a light-jet mimics a b-jet with a rate of 0.135% [78].

BPs [GeV]	The other input parameters
BP1 ($M_{H_F} = 300$)	$M_{A_F} = 300$ GeV, $\lambda_1 = 0.272$, $\lambda_2 = 0.089$, $\lambda_3 = 0.029$
BP2 ($M_{H_F} = 600$)	$M_{A_F} = 600$ GeV, $\lambda_1 = 0.316$, $\lambda_2 = 0.358$, $\lambda_3 = 0.138$
BP3 ($M_{H_F} = 900$)	$M_{A_F} = 900$ GeV, $\lambda_1 = 0.390$, $\lambda_2 = 0.806$, $\lambda_3 = 0.320$

TABLE II: The input parameters of the three BPs (BP1, BP2 and BP3) used in the remainder of the paper. We have $M_h = 125.5$ GeV, $\cos\alpha = 0.995$, $v_s = 1000$ GeV and $\Lambda_F = 1$ TeV is this kept fixed for all BPs.

BPs [GeV]	BRs and cross sections [pb]		
	BR($H_F \to hh$)	$\sigma(pp \to H_F)$	$\sigma(pp \to H_F \to hh, h \to \gamma\gamma, h \to b\bar{b})$
BP1 ($M_{H_F} = 300$)	0.351	9.033	4.088×10^{-3}
BP2 ($M_{H_F} = 600$)	0.118	1.837	2.805×10^{-4}
BP3 ($M_{H_F} = 900$)	0.147	0.209	3.952×10^{-5}

TABLE III: The BR($H_F \to hh$) and cross sections for the processes $pp \to H_F$ and $\sigma(pp \to H_F \to hh, h \to \gamma\gamma, h \to b\bar{b})$ for three BPs (BP1, BP2 and BP3) used in the remainder of the paper.

We next present a detailed discussion of the collider search strategy employed to maximize the signal significance in the search channel $pp \to H_F \to hh$ ($h \to \gamma\gamma, h \to b\bar{b}$). To start with, though, we show the production and decay cross section $pp \to H_F \to hh$ ($h \to \gamma\gamma, h \to b\bar{b}$) for the three BPs presented in Tab. II (with, in particular, $M_{H_F} = 300,\ 600$ and 900 GeV, as seen in Tab. III). The corresponding dominant SM backgrounds are shown in Tab. IV.

Any charged objects (leptons or jets) or photons produced in any hard scattering process at the LHC will be observed in the detector if and only if they satisfy certain geometric criteria,

SM backgrounds	Cross section [pb]
$pp \to b\bar{b}\gamma\gamma$	4.569
$pp \to Zh\,(Z \to b\bar{b}, h \to \gamma\gamma)$	1.394×10^{-4}
$pp \to b\bar{b}j\gamma$	7470.021
$pp \to b\bar{b}jj$	5.033×10^{6}
(j mimic as photon)	
$pp \to c\bar{c}\gamma\gamma$	6.215
$pp \to c\bar{c}j\gamma$	2085.012
(c appear as b-tagged jets,	
j mimic as photon)	
$pp \to jj\gamma\gamma$	65.231
(j appear as b-tagged jets)	
$pp \to t\bar{t}\,(t \to \bar{l}\nu_l b, \bar{t} \to l\bar{\nu}_l\bar{b})$	6.166×10^{-5}
$pp \to t\bar{t}\,(t \to jjb, \bar{t} \to jj\bar{b})$	202.151
(l, j mimic as photon)	

TABLE IV: The cross sections for the most relevant SM background processes. (Note that these background rates will be multiplied by the fake rates during the analysis.)

known as acceptance cuts. These are the same for both the signal and background events and reproduce the accessible region of the detector. We will then have to ask that both signal and background events pass these acceptance cuts, which are, in general, not sufficient to separate the two samples. However, eventually, we will construct various kinematic observables and study their distributions. Next, we will decide the final selection cuts after studying the distinguishing features of those distributions between signal and backgrounds, so as to increase the former and decrease the latter. We base this approach on a Monte Carlo (MC) analysis using the tools previously described.

In our current scenario, an event is required to have exactly two b-tagged jets and two isolated photons (γ) in the final state. However, we do not put any constraints on the number of light-jets. We then adopt the following acceptance cuts:

- $p_T^{\gamma} > 20$ GeV;
- $p_T^{e/\mu} > 20$ GeV (if an electron/muon is present, for b-tagging purposes);
- $p_T^{j} > 40$ GeV, where j stands for light-jets as well as b-jets;
- $|\,\eta_\ell\,| \leq 2.5$ (again, $\ell = e/\mu$), $|\,\eta_\gamma\,| \leq 2.0$ and $|\,\eta_j\,| \leq 2.0$.

After considering these basic requirements, we apply a stronger selection (using additional kinematic variables) in order to enhance the signal-to-background ratio, as explained. A variety of such observables have been used to design the optimized Signal Region (SR), i.e., where the

significance is maximized. First and foremost, the transverse momentum of photons ($p_T^{\gamma_1}$, $p_T^{\gamma_2}$) and b-jets ($p_T^{b_1}$, $p_T^{b_2}$)[3] will be studied. In addition, the separation between the two final state photons $\Delta R_{\gamma_1\gamma_2}$ and b-jets $\Delta R_{b_1 b_2}$ are also used. The separation between two detector objects, ΔR, is defined as $\Delta R = \sqrt{\Delta\eta^2 + \Delta\phi^2}$, where $\Delta\eta$ and $\Delta\phi$ are the differences in pseudorapidity and azimuthal angle, respectively. Then, the invariant mass of the final state photons ($M_{\gamma_1\gamma_2}$) and b-jets ($M_{b_1 b_2}$) will also be used to discriminate between signal and backgrounds, where we have introduced $M_{ab} = \sqrt{(E^a + E^b)^2 - \sum_{i=x,y,x}(p_i^a + p_i^b)^2}$, with $ab = \gamma_1\gamma_2$ or $b_1 b_2$. Finally, we use the invariant mass M_{hh} for the final extraction. The M_{hh} variable has been calculated as $M_{hh} = \sqrt{(E^{\gamma_1} + E^{\gamma_2} + E^{b_1} + E^{b_2})^2 - \sum_{i=x,y,z}(p_i^{\gamma_1} + p_i^{\gamma_2} + p_i^{b_1} + p_i^{b_2})^2}$. In the above formulae, E and p_i ($i = x, y, z$) stand for the energy and three-momentum component of the final state particles, respectively.

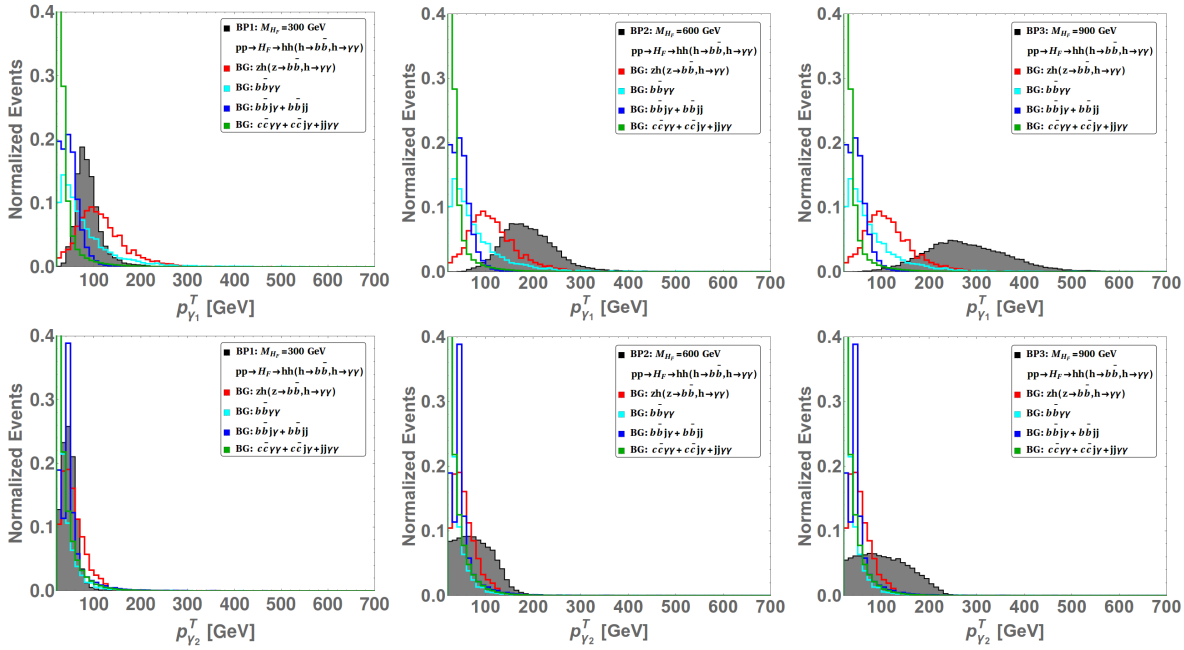

FIG. 8: Normalized distributions in photon transverse momentum for signal and total background after the acceptance cuts.

The (arbitrarily) normalized distributions of all these kinematic variables for the three signal BPs and the total background are shown in Figs. 8–12. Based on their inspection, as intimated, we then perform a detailed cut-based analysis to maximize the signal significance against the background. The sequence of constraints adopted is shown in Tab. V. Specifically, notice that, in applying the last requirement herein (on the M_{hh} variable), one may assume that the M_{H_F} value is a trial one, if it were not already known from previous analysis.

The signal yields for BP1, BP2 and BP3, along with the corresponding background ones,

[3] Here, 1 and 2 represents the p_T ordered leading and sub-leading photon and b-jet in the final state.

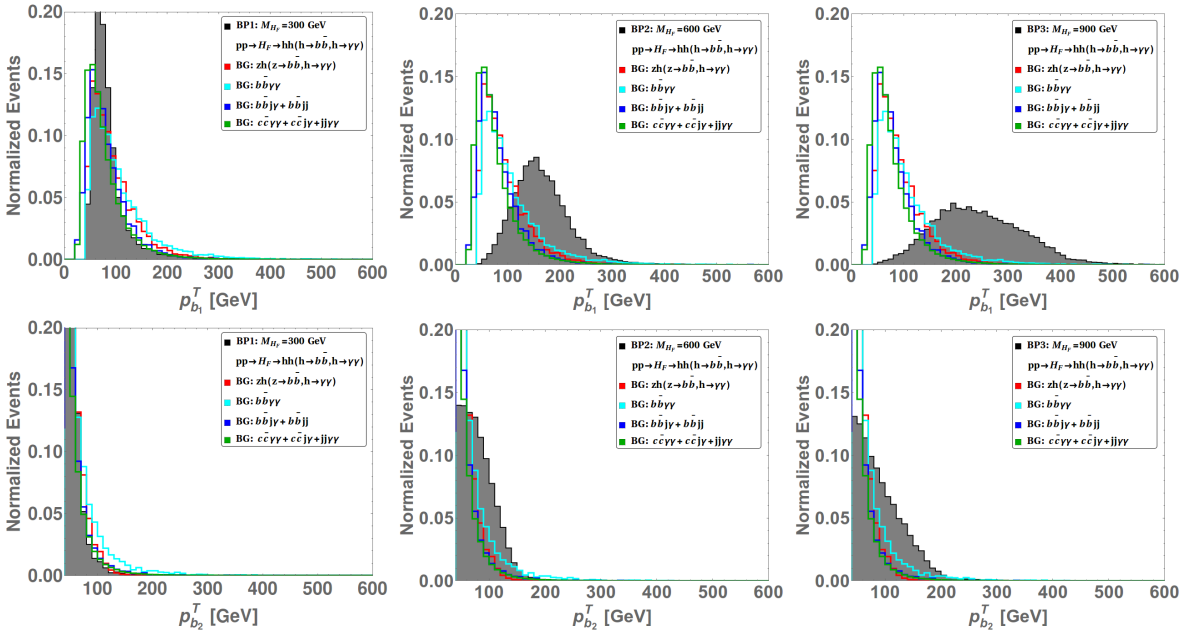

FIG. 9: Normalized distributions in b-jet transverse momentum for signal and total background after the acceptance cuts.

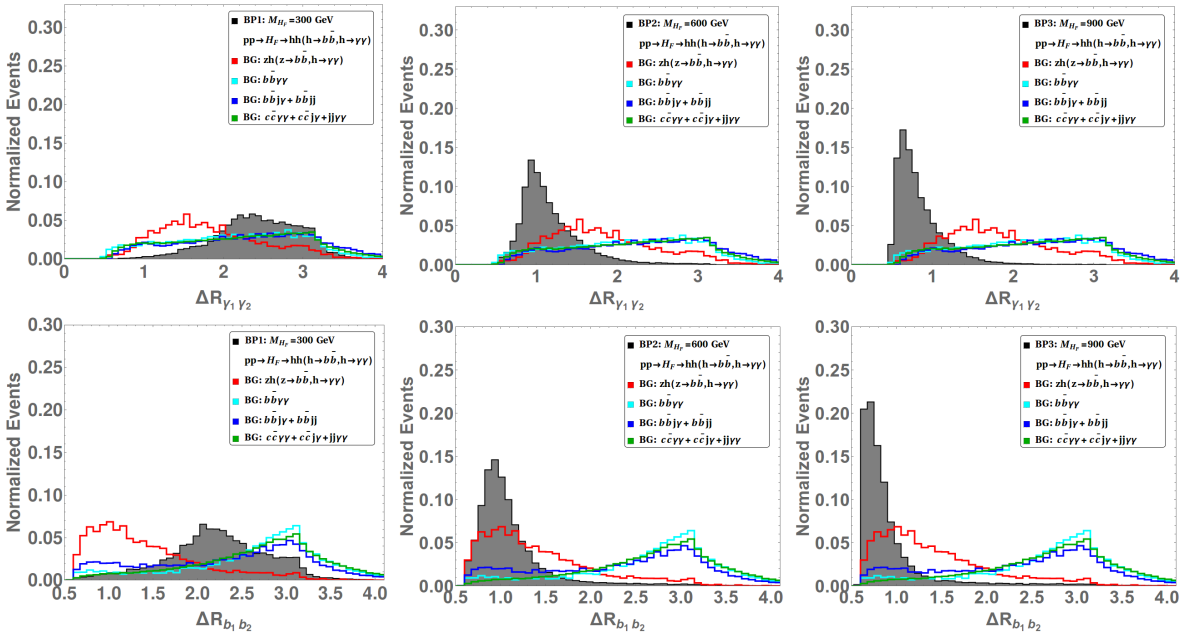

FIG. 10: Normalized distributions in di-photon and di-jet separation for signal and total background after the acceptance cuts.

obtained after the application of the acceptance and selection cuts defining the SR, are shown in Tab. VI for $\sqrt{s} = 14$ TeV and, e.g., $\mathcal{L} = 3000$ fb^{-1}. We initially calculate the signal significance using the relation $\sigma = \frac{S}{\sqrt{S+B}}$. Here, S and B stand for the Signal and (total SM) Background

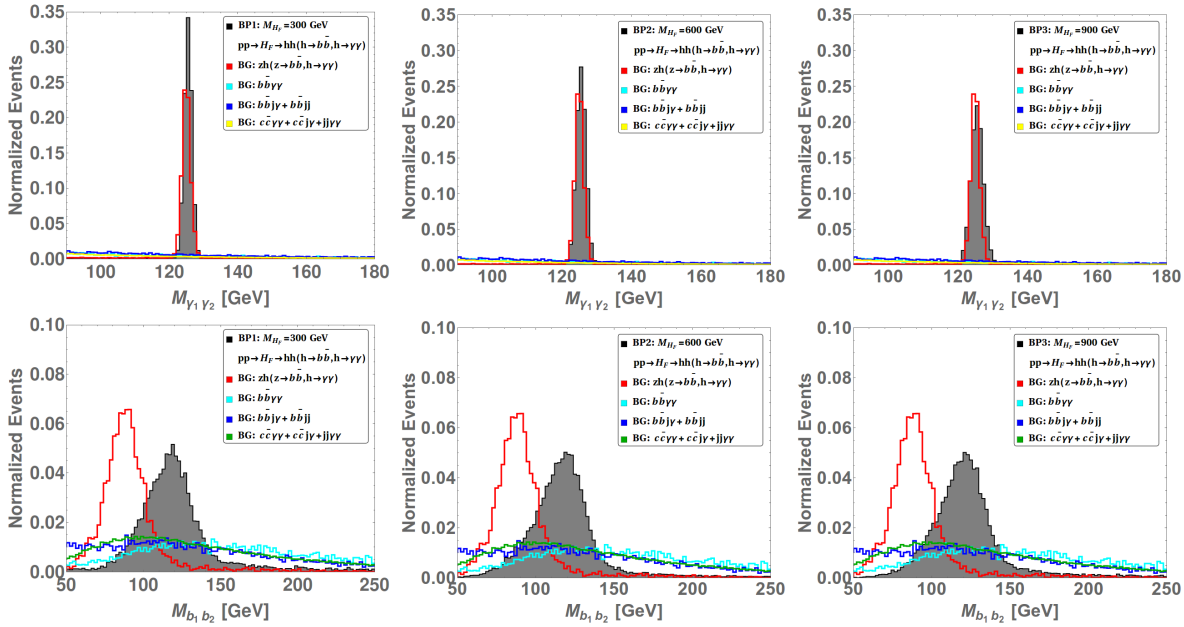

FIG. 11: Normalized distributions in di-photon and di-jet invariant mass for signal and total background after the acceptance cuts.

	Kinematic variables and cuts	
	Observable	Value
SR	$p_T^{\gamma_{1,2}}$	> 35.0 (GeV)
	$p_T^{b_{1,2}}$	> 40.0 (GeV)
	$M_{\gamma_1\gamma_2}$	$122.5 - 128.5$ (GeV)
	$M_{b_1 b_2}$	$70.0 - 135.0$ (GeV)
	$\Delta R_{\gamma_1\gamma_2}$	$0.4 - 4.6$
	$\Delta R_{b_1 b_2}$	$0.4 - 3.6$
	M_{hh} (varied with M_{H_F})	$0.7M_{H_F} - 1.1M_{H_F}$

TABLE V: The optimized SR as a function of the H_F mass.

rates, respectively. The number of S and B events is obtained as $S, B = \epsilon A \sigma_{S,B} \mathcal{L}$, where ϵ and A stand for the selection and acceptance cut efficiency, respectively, $\sigma_{S,B}$ is the S or B cross section and $\mathcal{L}$ is the luminosity. Based on these definitions, it is clear from Tab. VI that strong HL-LHC sensitivity exists for all M_{H_F} choices, ranging from discovery (at small masses) to exclusion (at high masses). (It should be appreciated that these significances would be reduced by as much as 30% in the absence of the final M_{hh} selection.) In fact, one can also consider the systematic uncertainty in various SM background estimations while calculating the final signal significance

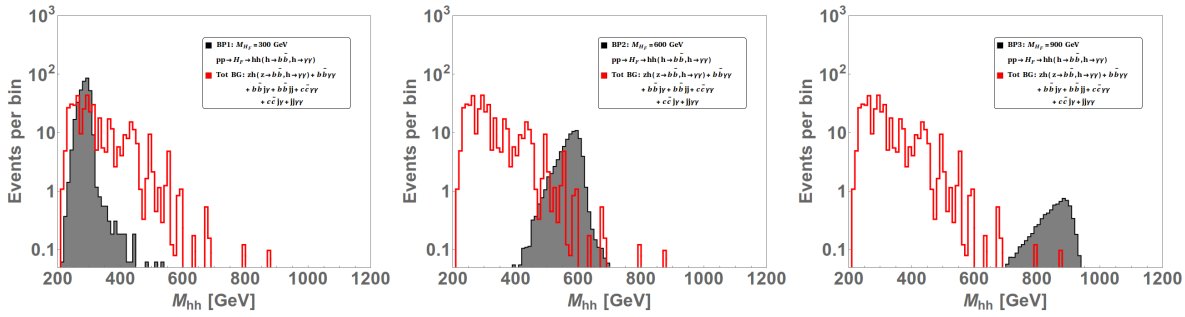

FIG. 12: Distributions in the final state invariant mass for signal and total background after the acceptance cuts as well as the selection ones on $p_T^{\gamma_{1,2}}$, $p_T^{b_{1,2}}$, $M_{\gamma_1\gamma_2}$, $M_{b_1b_2}$, $\Delta R_{\gamma_1\gamma_2}$ and $\Delta R_{b_1b_2}$, as shown in Tab. V.

as[4] $\sigma = \frac{S}{\sqrt{S+B+(\kappa B)^2}}$, where κ is the percentage of systematic uncertainty [79]. Upon adding 5% for the latter, the significance in Tab. VI for BP1 decreases to 12.35 while for BP2 and BP3 it becomes 6.65 and 2.31, respectively. Hence, the HL-LHC sensitivity is very stable against unknowns affecting the data sample estimations, whatever the origin.

Benchmark points: Signal and Significances								
BP1 ($M_{H_F} = 300$ GeV)			BP2 ($M_{H_F} = 600$ GeV)			BP3 ($M_{H_F} = 900$ GeV)		
# Signal	# Background	Significance	# Signal	# Background	Significance	# Signal	# Background	Significance
332.338	255.047	13.71	75.994	48.471	6.81	7.916	3.717	2.32

TABLE VI: The signal significance $\sigma = \frac{S}{\sqrt{S+B}}$ for BP1, BP2 and BP3 corresponding to the optimized SR are shown. In addition, the total background yield and the total signal yield are also given at $\sqrt{s} = 14$ TeV with integrated luminosity $\mathcal{L} = 3000$ fb^{-1}.

In Fig. 13 (upper-left panel), we present the significances as a continuous distribution in M_{H_F}, from to 250 to 1000 GeV. It is to be noted that this reaches a maximum at $M_{H_F} = 2M_t$, where $M_t = 173.1$ GeV is the top quark mass, corresponding to the threshold in the loop function. Notice that in Fig. 13 (upper-right panel) we also show the significances for $\mathcal{L} = 300$ fb^{-1}, so as to highlight the rather substantial scope of Run 3 of the LHC. In the lower panels of Fig. 13, a $\kappa = 5\%$ systematic uncertainty has been taken into account, yielding very moderate corrections.

We now derive the various projected limits over the $M_{H_F} - v_s$ plane. It is to be noted that the variation of the singlet scalar VEV v_s will directly change the $H_F hh$ coupling and correspondingly the production cross section $\sigma(pp \to H_F \to hh)$. In particular, the smaller the former the larger

[4] To include the systematic uncertainty in $\sigma = \frac{S}{\sqrt{S+B}}$, one can replace $S+B$ in the denominator by the quadratic sum of $\sqrt{S+B}$ and use $\sigma_b = \kappa B$ [79], i.e., $\sigma = \frac{S}{\sqrt{S+B+(\kappa B)^2}}$, with κ being the percentage of systematic uncertainty of the total background.

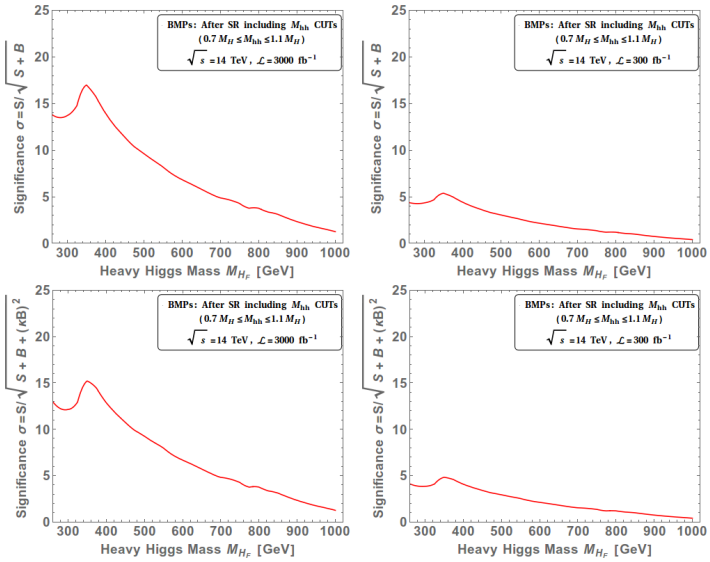

FIG. 13: The signal significances with integrated luminosity 3000 and 300 fb^{-1} respectively. The lower panel plots are drawn considering a systematic uncertainty $\kappa = 5\%$.

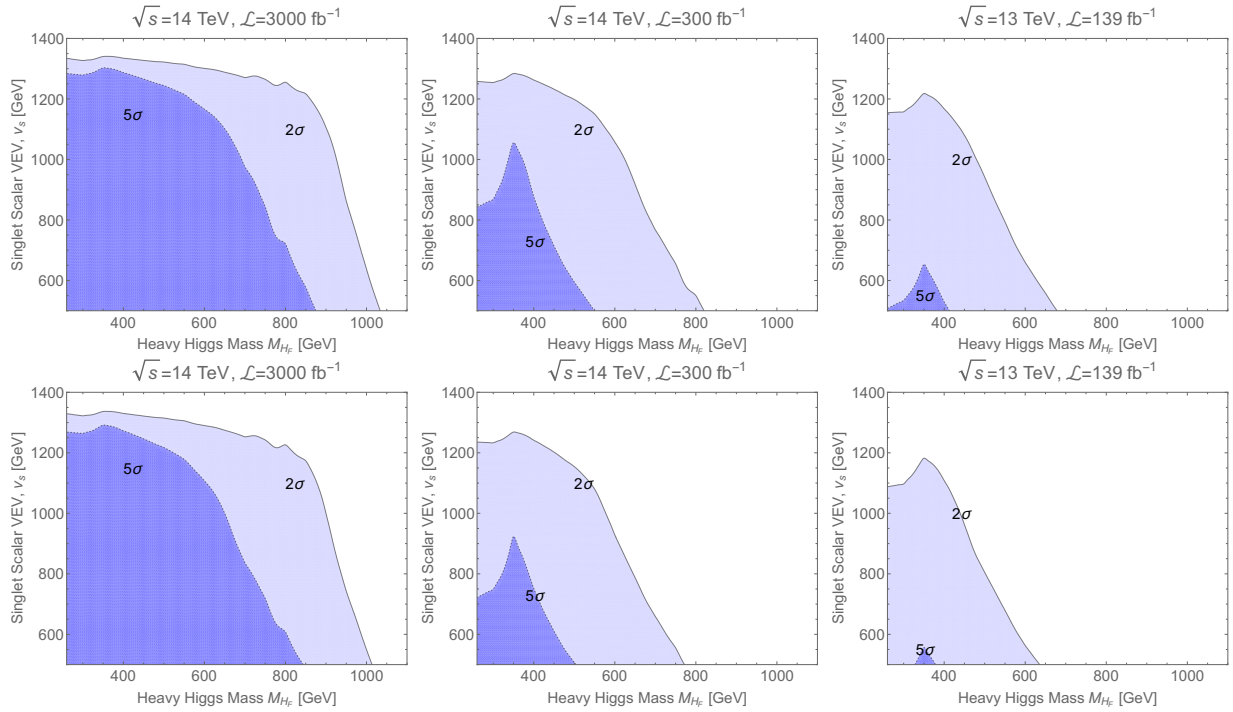

FIG. 14: The projected exclusion (light blue) and discovery (dark blue) regions in the $M_{H_F} - v_s$ plane. The left and middle plots are drawn for $\mathcal{L} = 3000$ and 300 fb^{-1}, respectively. The right plot represents the current limits in the context of the ATLAS analysis with $\sqrt{s} = 13$ TeV and $\mathcal{L} = 139$ fb^{-1}. The lower panel plots are drawn considering a systematic uncertainty $\kappa = 5\%$.

the latter. To accurately delineate sensitivity regions, we generate a large number of signal

events for various combinations of heavy CP-even Flavon mass, M_{H_F}, and singlet scalar VEV, v_s. Specifically, $M_{H_F}(= M_{A_F})$ has been varied from 260 GeV to 1000 GeV with a step size of 10 GeV while v_s has been varied between 500 and 1000 GeV with a step size of 50 GeV. The projected exclusion (2σ) and discovery (5σ) regions derived from the $\gamma\gamma b\bar{b}$ final state in the $M_{H_F} - v_s$ plane are given in Fig. 14, where they have been represented in light blue and dark blue colors, respectively. The left and middle plots are drawn for $\mathcal{L} = 3000$ fb^{-1} (HL-LHC) and 300 fb^{-1} (Run 3), respectively. Alongside these, we also report (right plots) the corresponding results obtained assuming the ATLAS Collaboration data sample at Run 2 ($\sqrt{s} = 13$ TeV and $\mathcal{L} = 139$ fb^{-1}) but using our dedicated selection. The results in this figure reinforce those in the previous ones by illustrating the strong sensitivity of the HL-LHC to the advocated FNSM signal over a significant portion of its parameter space while also highlighting the appreciable scope of Run 3. (Indeed, a kinematical re-analysis of Run 2 samples along the lines developed here may also prove to have moderate sensitivity.) Again, the plots in the upper panels of Fig. 14 are shown with no systematic uncertainty, i.e., $\kappa = 0$, while those in the lower panels are drawn based on a systematic uncertainty $\kappa = 5\%$. From the top row of plots, it can be observed that, for $v_s = 500$ GeV, at 14 TeV with 3000 fb^{-1}, the direct search for the H_F mediated $\gamma\gamma b\bar{b}$ signal has a potential discovery (exclusion) reach up to $M_{H_F} \approx 900$ GeV (1050 GeV) while this is reduced to $M_{H_F} \approx 570$ GeV (820 GeV) for a luminosity of 300 fb^{-1}. (The discussed potential exclusion limit from the present ATLAS Collaboration data would reach up to ~ 700 GeV while the region below ~ 400 GeV would be excluded in the presence of a non-observation.) From the bottom row of plots, we should mention that the mentioned limits drop somewhat (by $5 - 10\%$) upon introducing a systematic uncertainty of $\kappa = 5\%$, hence not too drastic a reduction of sensitivity in general (as already remarked for our BPs).

V. CONCLUSIONS

The hierarchical structure and peculiar pattern of quark and lepton masses in the SM have been a long standing issue coined as the 'flavor puzzle'. Various interesting beyond the SM proposals have been suggested to resolve this riddle. Among these, the one by Froggatt and Nielsen is arguably one of the most fascinating ones. Herein, the scalar sector predicts one singlet complex scalar S_F which is charged under a new $U(1)_F$ flavor symmetry (which is softly broken). After EWSB and $U(1)_F$ breaking, the mixing between the SM Higgs doublet with the real part of the S_F singlet produces two physical scalars, h and H_F, where h is identified as the SM-like Higgs boson (discovered in 2012) while H_F is an additional CP-even (so-called) Flavon with mass $\mathcal{O}(1$ TeV). (The imaginary part of S_F is identified as the CP-odd heavy Flavon A_F.) The (pseudo)scalar sector of this model is controlled by two parameters: the Flavon VEV v_s and the mixing angle α. The structure of various Yukawa couplings of this model is such that one can have Flavor Changing Neutral Currents (FCNCs) involving the two new heavy (pseudo)scalars ($H_F\&A_F$) even at tree-level. The corresponding contributions to FCNC processes thus attract

severe constraints from various low energy flavor physics data. Therefore, in our analysis of such a scenario, we have considered all possible experimental (as well as theoretical) limits on the model parameters v_s and α. With the LHC currently running at CERN, it is very tempting to utilize the ongoing (Run 3) and future (HL-LHC) stages of the machine to explore the signature of such heavy flavons.

In this paper, we have focused on the CP-even heavy Flavon H_F and made some predictions on its discovery potential at the LHC through its production via gluon-gluon fusion followed by its decay into pairs of SM Higgs bosons. We have shown that, for certain choices of M_{H_F}, the BR($H_F \to hh$) can be large enough so that the whole process $pp \to H_F \to hh$ ($h \to \gamma\gamma, h \to b\bar{b}$) can be probed at both Run 3 and HL-LHC (with $\sqrt{s} = 14$ TeV), assuming 300 fb^{-1} and 3000 fb^{-1} of luminosity, respectively, through either exclusion or discovery.

We have obtained such a result following a thorough numerical analysis emulating both the aforementioned signal and the most relevant (ir)reducible backgrounds accounting for hard scattering, parton shower, hadronization and detector effects. We thus advocate that the experimental collaborations at the LHC, specifically, the multipurpose ones (ATLAS and CMS), tackle this search, as its results can lead to a better understanding of the origin and solution of the flavor puzzle in the SM. This should be facilitated by having implemented the advocated model in standard computational tools, which are available upon request.

Acknowledgments

SM acknowledges funding from the STFC Consolidated Grant ST/L000296/1 and is partially supported through the NExT Institute. NK would like to acknowledge support from the DAE, Government of India and the Regional Centre for Accelerator-based Particle Physics (RECAPP), HRI. The work of MAA-U is supported by the Centro Interdisciplinario de Investigación y Enseñanza de la Ciencia (CIIEC). JLD-C acknowledges the support of SNI (México) and VIEP (BUAP). The work of AC is funded by the Department of Science and Technology, Government of India, under Grant No. IFA18PH224 (INSPIRE Faculty Award).

---

[1] **ATLAS** Collaboration, G. Aad *et al.*, "Observation of a new particle in the search for the Standard Model Higgs boson with the ATLAS detector at the LHC," *Phys. Lett. B* **716** (2012) 1–29, arXiv:1207.7214 [hep-ex].

[2] **CMS** Collaboration, S. Chatrchyan *et al.*, "Observation of a New Boson at a Mass of 125 GeV with the CMS Experiment at the LHC," *Phys. Lett. B* **716** (2012) 30–61, arXiv:1207.7235 [hep-ex].

[3] P. P. Giardino, K. Kannike, I. Masina, M. Raidal, and A. Strumia, "The universal Higgs fit," *JHEP* **05** (2014) 046, arXiv:1303.3570 [hep-ph].

[4] **CMS** Collaboration, A. M. Sirunyan *et al.*, "Observation of the Higgs boson decay to a pair of τ leptons with the CMS detector," *Phys. Lett.* **B779** (2018) 283–316, arXiv:1708.00373 [hep-ex].

[5] **CMS** Collaboration, A. M. Sirunyan *et al.*, "Combined measurements of Higgs boson couplings in proton–proton collisions at $\sqrt{s} = 13\,\text{TeV}$," *Eur. Phys. J.* **C79** no. 5, (2019) 421, arXiv:1809.10733 [hep-ex].

[6] Z. Kunszt, S. Moretti, and W. J. Stirling, "Higgs production at the LHC: An Update on cross-sections and branching ratios," *Z. Phys. C* **74** (1997) 479–491, arXiv:hep-ph/9611397.

[7] S. Dawson, S. Dittmaier, and M. Spira, "Neutral Higgs boson pair production at hadron colliders: QCD corrections," *Phys. Rev. D* **58** (1998) 115012, arXiv:hep-ph/9805244.

[8] J. Baglio, F. Campanario, S. Glaus, M. Mühlleitner, M. Spira, and J. Streicher, "Gluon fusion into Higgs pairs at NLO QCD and the top mass scheme," *Eur. Phys. J. C* **79** no. 6, (2019) 459, arXiv:1811.05692 [hep-ph].

[9] J. Baglio, F. Campanario, S. Glaus, M. Mühlleitner, J. Ronca, M. Spira, and J. Streicher, "Higgs-Pair Production via Gluon Fusion at Hadron Colliders: NLO QCD Corrections," *JHEP* **04** (2020) 181, arXiv:2003.03227 [hep-ph].

[10] J. Baglio, A. Djouadi, R. Gröber, M. M. Mühlleitner, J. Quevillon, and M. Spira, "The measurement of the Higgs self-coupling at the LHC: theoretical status," *JHEP* **04** (2013) 151, arXiv:1212.5581 [hep-ph].

[11] V. Barger, L. L. Everett, C. B. Jackson, and G. Shaughnessy, "Higgs-Pair Production and Measurement of the Triscalar Coupling at LHC(8,14)," *Phys. Lett. B* **728** (2014) 433–436, arXiv:1311.2931 [hep-ph].

[12] N. Kumar and S. P. Martin, "LHC search for di-Higgs decays of stoponium and other scalars in events with two photons and two bottom jets," *Phys. Rev. D* **90** no. 5, (2014) 055007, arXiv:1404.0996 [hep-ph].

[13] A. Adhikary, S. Banerjee, R. Kumar Barman, and B. Bhattacherjee, "Resonant heavy Higgs searches at the HL-LHC," *JHEP* **09** (2019) 068, arXiv:1812.05640 [hep-ph].

[14] A. Adhikary, S. Banerjee, R. K. Barman, B. Bhattacherjee, and S. Niyogi, "Revisiting the non-resonant Higgs pair production at the HL-LHC," *JHEP* **07** (2018) 116, arXiv:1712.05346 [hep-ph].

[15] A. Adhikary, R. K. Barman, and B. Bhattacherjee, "Prospects of non-resonant di-Higgs searches and Higgs boson self-coupling measurement at the HE-LHC using machine learning techniques," *JHEP* **12** (2020) 179, arXiv:2006.11879 [hep-ph].

[16] J. Baglio, O. Eberhardt, U. Nierste, and M. Wiebusch, "Benchmarks for Higgs Pair Production and Heavy Higgs boson Searches in the Two-Higgs-Doublet Model of Type II," *Phys. Rev. D* **90** no. 1, (2014) 015008, arXiv:1403.1264 [hep-ph].

[17] B. Hespel, D. Lopez-Val, and E. Vryonidou, "Higgs pair production via gluon fusion in the Two-Higgs-Doublet Model," *JHEP* **09** (2014) 124, arXiv:1407.0281 [hep-ph].

[18] L.-C. Lü, C. Du, Y. Fang, H.-J. He, and H. Zhang, "Searching heavier Higgs boson via di-Higgs

production at LHC Run-2," *Phys. Lett. B* **755** (2016) 509–522, arXiv:1507.02644 [hep-ph].

[19] G. D. Kribs and A. Martin, "Enhanced di-Higgs Production through Light Colored Scalars," *Phys. Rev. D* **86** (2012) 095023, arXiv:1207.4496 [hep-ph].

[20] L. Bian and N. Chen, "Higgs pair productions in the CP-violating two-Higgs-doublet model," *JHEP* **09** (2016) 069, arXiv:1607.02703 [hep-ph].

[21] S. Dawson, E. Furlan, and I. Lewis, "Unravelling an extended quark sector through multiple Higgs production?," *Phys. Rev. D* **87** no. 1, (2013) 014007, arXiv:1210.6663 [hep-ph].

[22] A. Pierce, J. Thaler, and L.-T. Wang, "Disentangling Dimension Six Operators through Di-Higgs Boson Production," *JHEP* **05** (2007) 070, arXiv:hep-ph/0609049.

[23] S. Kanemura and K. Tsumura, "Effects of the anomalous Higgs couplings on the Higgs boson production at the Large Hadron Collider," *Eur. Phys. J. C* **63** (2009) 11–21, arXiv:0810.0433 [hep-ph].

[24] U. Ellwanger, "Higgs pair production in the NMSSM at the LHC," *JHEP* **08** (2013) 077, arXiv:1306.5541 [hep-ph].

[25] C.-R. Chen and I. Low, "Double take on new physics in double Higgs boson production," *Phys. Rev. D* **90** no. 1, (2014) 013018, arXiv:1405.7040 [hep-ph].

[26] N. Liu, S. Hu, B. Yang, and J. Han, "Impact of top-Higgs couplings on Di-Higgs production at future colliders," *JHEP* **01** (2015) 008, arXiv:1408.4191 [hep-ph].

[27] F. Goertz, A. Papaefstathiou, L. L. Yang, and J. Zurita, "Higgs boson pair production in the D=6 extension of the SM," *JHEP* **04** (2015) 167, arXiv:1410.3471 [hep-ph].

[28] A. Azatov, R. Contino, G. Panico, and M. Son, "Effective field theory analysis of double Higgs boson production via gluon fusion," *Phys. Rev. D* **92** no. 3, (2015) 035001, arXiv:1502.00539 [hep-ph].

[29] M. J. Dolan, C. Englert, and M. Spannowsky, "New Physics in LHC Higgs boson pair production," *Phys. Rev. D* **87** no. 5, (2013) 055002, arXiv:1210.8166 [hep-ph].

[30] V. Barger, L. L. Everett, C. B. Jackson, A. D. Peterson, and G. Shaughnessy, "New physics in resonant production of Higgs boson pairs," *Phys. Rev. Lett.* **114** no. 1, (2015) 011801, arXiv:1408.0003 [hep-ph].

[31] A. Crivellin, M. Ghezzi, and M. Procura, "Effective Field Theory with Two Higgs Doublets," *JHEP* **09** (2016) 160, arXiv:1608.00975 [hep-ph].

[32] H. Sun, Y.-J. Zhou, and H. Chen, "Constraints on large-extra-dimensions model through 125-GeV Higgs pair production at the LHC," *Eur. Phys. J. C* **72** (2012) 2011, arXiv:1211.5197 [hep-ph].

[33] R. Costa, M. Mühlleitner, M. O. P. Sampaio, and R. Santos, "Singlet Extensions of the Standard Model at LHC Run 2: Benchmarks and Comparison with the NMSSM," *JHEP* **06** (2016) 034, arXiv:1512.05355 [hep-ph].

[34] K. Cheung, A. Jueid, C.-T. Lu, J. Song, and Y. W. Yoon, "Disentangling new physics effects on nonresonant Higgs boson pair production from gluon fusion," *Phys. Rev. D* **103** no. 1, (2021) 015019, arXiv:2003.11043 [hep-ph].

[35] A. Alves, D. Gonçalves, T. Ghosh, H.-K. Guo, and K. Sinha, "Di-Higgs Production in the $4b$ Channel and Gravitational Wave Complementarity," *JHEP* **03** (2020) 053, arXiv:1909.05268 [hep-ph].

[36] C. Englert and J. Jaeckel, "Probing the Symmetric Higgs Portal with Di-Higgs Boson Production," *Phys. Rev. D* **100** no. 9, (2019) 095017, arXiv:1908.10615 [hep-ph].

[37] P. Basler, S. Dawson, C. Englert, and M. Mühlleitner, "Showcasing HH production: Benchmarks for the LHC and HL-LHC," *Phys. Rev. D* **99** no. 5, (2019) 055048, arXiv:1812.03542 [hep-ph].

[38] Z. Heng, X. Gong, and H. Zhou, "Pair production of Higgs boson in NMSSM at the LHC with the next-to-lightest CP-even Higgs boson being SM-like," *Chin. Phys. C* **42** no. 7, (2018) 073103, arXiv:1805.01598 [hep-ph].

[39] B. Das, S. Moretti, S. Munir, and P. Poulose, "Quantum interference effects in Higgs boson pair-production beyond the Standard Model," *Eur. Phys. J. C* **81** no. 4, (2021) 347, arXiv:2012.09587 [hep-ph].

[40] H. Abouabid, A. Arhrib, D. Azevedo, J. E. Falaki, P. M. Ferreira, M. Mühlleitner, and R. Santos, "Benchmarking Di-Higgs Production in Various Extended Higgs Sector Models," arXiv:2112.12515 [hep-ph].

[41] S. Dasgupta, R. Pramanick, and T. S. Ray, "Broad toplike vector quarks at LHC and HL-LHC," *Phys. Rev. D* **105** no. 3, (2022) 035032, arXiv:2112.03742 [hep-ph].

[42] L. Huang, S.-b. Kang, J. H. Kim, K. Kong, and J. S. Pi, "Portraying Double Higgs at the Large Hadron Collider II," arXiv:2203.11951 [hep-ph].

[43] C. D. Froggatt and H. B. Nielsen, "Hierarchy of Quark Masses, Cabibbo Angles and CP Violation," *Nucl. Phys. B* **147** (1979) 277–298.

[44] A. Bolaños, J. L. Diaz-Cruz, G. Hernández-Tomé, and G. Tavares-Velasco, "Has a Higgs-flavon with a 750 GeV mass been detected at the LHC13?," *Phys. Lett. B* **761** (2016) 310–317, arXiv:1604.04822 [hep-ph].

[45] M. Bauer, T. Schell, and T. Plehn, "Hunting the Flavon," *Phys. Rev. D* **94** no. 5, (2016) 056003, arXiv:1603.06950 [hep-ph].

[46] K. Huitu, V. Keus, N. Koivunen, and O. Lebedev, "Higgs-flavon mixing and $h \to \mu\tau$," *JHEP* **05** (2016) 026, arXiv:1603.06614 [hep-ph].

[47] E. L. Berger, S. B. Giddings, H. Wang, and H. Zhang, "Higgs-flavon mixing and LHC phenomenology in a simplified model of broken flavor symmetry," *Phys. Rev. D* **90** no. 7, (2014) 076004, arXiv:1406.6054 [hep-ph].

[48] J. L. Diaz-Cruz and U. J. Saldaña Salazar, "Higgs couplings and new signals from Flavon–Higgs mixing effects within multi-scalar models," *Nucl. Phys. B* **913** (2016) 942–963, arXiv:1405.0990 [hep-ph].

[49] M. A. Arroyo-Ureña, J. L. Díaz-Cruz, G. Tavares-Velasco, A. Bolaños, and G. Hernández-Tomé, "Searching for lepton flavor violating flavon decays at hadron colliders," *Phys. Rev. D* **98** no. 1, (2018) 015008, arXiv:1801.00839 [hep-ph].

[50] M. A. Arroyo-Ureña, A. Fernández-Téllez, and G. Tavares-Velasco, "Flavor changing Flavon decay $\phi \to tc$ ($\phi = H_F$, A_F) at the high-luminosity large hadron collider," arXiv:1906.07821 [hep-ph].

[51] F. Gianotti *et al.*, "Physics potential and experimental challenges of the LHC luminosity upgrade," *Eur. Phys. J. C* **39** (2005) 293–333, arXiv:hep-ph/0204087.

[52] G. Apollinari, O. Brüning, T. Nakamoto, and L. Rossi, "High Luminosity Large Hadron Collider HL-LHC," *CERN Yellow Rep.* no. 5, (2015) 1–19, arXiv:1705.08830 [physics.acc-ph].

[53] **ATLAS** Collaboration, G. Aad *et al.*, "Combination of searches for Higgs boson pairs in pp collisions at $\sqrt{s}$ =13 TeV with the ATLAS detector," *Phys. Lett. B* **800** (2020) 135103, arXiv:1906.02025 [hep-ex].

[54] **ATLAS** Collaboration, M. Aaboud *et al.*, "Search for Higgs boson pair production in the $WW^{(*)}WW^{(*)}$ decay channel using ATLAS data recorded at $\sqrt{s} = 13$ TeV," *JHEP* **05** (2019) 124, arXiv:1811.11028 [hep-ex].

[55] **ATLAS** Collaboration, M. Aaboud *et al.*, "Search for Higgs boson pair production in the $b\bar{b}WW^*$ decay mode at $\sqrt{s} = 13$ TeV with the ATLAS detector," *JHEP* **04** (2019) 092, arXiv:1811.04671 [hep-ex].

[56] **ATLAS** Collaboration, M. Aaboud *et al.*, "Search for resonant and non-resonant Higgs boson pair production in the $b\bar{b}\tau^+\tau^-$ decay channel in pp collisions at $\sqrt{s} = 13$ TeV with the ATLAS detector," *Phys. Rev. Lett.* **121** no. 19, (2018) 191801, arXiv:1808.00336 [hep-ex]. [Erratum: Phys.Rev.Lett. 122, 089901 (2019)].

[57] **CMS** Collaboration, A. M. Sirunyan *et al.*, "Search for Higgs boson pair production in events with two bottom quarks and two tau leptons in proton–proton collisions at $\sqrt{s}$ =13TeV," *Phys. Lett. B* **778** (2018) 101–127, arXiv:1707.02909 [hep-ex].

[58] **ATLAS** Collaboration, M. Aaboud *et al.*, "Search for Higgs boson pair production in the $\gamma\gamma WW^*$ channel using pp collision data recorded at $\sqrt{s} = 13$ TeV with the ATLAS detector," *Eur. Phys. J. C* **78** no. 12, (2018) 1007, arXiv:1807.08567 [hep-ex].

[59] **ATLAS** Collaboration, M. Aaboud *et al.*, "Search for Higgs boson pair production in the $\gamma\gamma b\bar{b}$ final state with 13 TeV pp collision data collected by the ATLAS experiment," *JHEP* **11** (2018) 040, arXiv:1807.04873 [hep-ex].

[60] **ATLAS** Collaboration, M. Aaboud *et al.*, "Search for pair production of Higgs bosons in the $b\bar{b}b\bar{b}$ final state using proton-proton collisions at $\sqrt{s} = 13$ TeV with the ATLAS detector," *JHEP* **01** (2019) 030, arXiv:1804.06174 [hep-ex].

[61] **CMS** Collaboration, A. M. Sirunyan *et al.*, "Combination of searches for Higgs boson pair production in proton-proton collisions at $\sqrt{s} = 13$ TeV," *Phys. Rev. Lett.* **122** no. 12, (2019) 121803, arXiv:1811.09689 [hep-ex].

[62] **ATLAS** Collaboration, "Constraints on the Higgs boson self-coupling from the combination of single-Higgs and double-Higgs production analyses performed with the ATLAS experiment,".

[63] C. Bonilla, D. Sokolowska, N. Darvishi, J. L. Diaz-Cruz, and M. Krawczyk, "IDMS: Inert Dark Matter Model with a complex singlet," *J. Phys. G* **43** no. 6, (2016) 065001, arXiv:1412.8730

[hep-ph].

[64] E. Barradas-Guevara, J. L. Diaz-Cruz, O. Félix-Beltrán, and U. J. Saldana-Salazar, "Linking LFV Higgs decays $h \to \ell_i \ell_j$ with CP violation in multi-scalar models," arXiv:1706.00054 [hep-ph].

[65] N. Khan and S. Rakshit, "Study of electroweak vacuum metastability with a singlet scalar dark matter," *Phys. Rev. D* **90** no. 11, (2014) 113008, arXiv:1407.6015 [hep-ph].

[66] G. Cynolter, E. Lendvai, and G. Pocsik, "Note on unitarity constraints in a model for a singlet scalar dark matter candidate," *Acta Phys. Polon. B* **36** (2005) 827–832, arXiv:hep-ph/0410102.

[67] M. Cepeda *et al.*, "Report from Working Group 2: Higgs Physics at the HL-LHC and HE-LHC," *CERN Yellow Rep. Monogr.* **7** (2019) 221–584, arXiv:1902.00134 [hep-ph].

[68] M. A. Arroyo-Ureña, R. Gaitán, and T. A. Valencia-Pérez, "SpaceMath version 1.0 A Mathematica package for beyond the standard model parameter space searches," *Rev. Mex. Fis. E* **19** no. 2, (2022) 020206, arXiv:2008.00564 [hep-ph].

[69] "Search for elusive "di-higgs production" reaches new milestone." https://atlas.cern/updates/briefing/new-milestone-di-Higgs-search.

[70] **ATLAS** Collaboration, G. Aad *et al.*, "Search for heavy resonances decaying into a pair of Z bosons in the $\ell^+\ell^-\ell'^+\ell'^-$ and $\ell^+\ell^-\nu\bar{\nu}$ final states using 139 fb^{-1} of proton–proton collisions at $\sqrt{s} = 13$ TeV with the ATLAS detector," *Eur. Phys. J. C* **81** no. 4, (2021) 332, arXiv:2009.14791 [hep-ex].

[71] **CMS** Collaboration, A. M. Sirunyan *et al.*, "Search for a heavy Higgs boson decaying to a pair of W bosons in proton-proton collisions at $\sqrt{s} = 13$ TeV," *JHEP* **03** (2020) 034, arXiv:1912.01594 [hep-ex].

[72] A. Alloul, N. D. Christensen, C. Degrande, C. Duhr, and B. Fuks, "FeynRules 2.0 - A complete toolbox for tree-level phenomenology," *Comput. Phys. Commun.* **185** (2014) 2250–2300, arXiv:1310.1921 [hep-ph].

[73] J. Alwall, R. Frederix, S. Frixione, V. Hirschi, F. Maltoni, O. Mattelaer, H. S. Shao, T. Stelzer, P. Torrielli, and M. Zaro, "The automated computation of tree-level and next-to-leading order differential cross sections, and their matching to parton shower simulations," *JHEP* **07** (2014) 079, arXiv:1405.0301 [hep-ph].

[74] T. Sjöstrand, S. Ask, J. R. Christiansen, R. Corke, N. Desai, P. Ilten, S. Mrenna, S. Prestel, C. O. Rasmussen, and P. Z. Skands, "An introduction to PYTHIA 8.2," *Comput. Phys. Commun.* **191** (2015) 159–177, arXiv:1410.3012 [hep-ph].

[75] **DELPHES 3** Collaboration, J. de Favereau, C. Delaere, P. Demin, A. Giammanco, V. Lemaître, A. Mertens, and M. Selvaggi, "DELPHES 3, A modular framework for fast simulation of a generic collider experiment," *JHEP* **02** (2014) 057, arXiv:1307.6346 [hep-ex].

[76] T. Plehn, "Lectures on LHC Physics," *Lect. Notes Phys.* **844** (2012) 1–193, arXiv:0910.4182 [hep-ph].

[77] **ATLAS** Collaboration, "Performance assumptions based on full simulation for an upgraded ATLAS detector at a High-Luminosity LHC," *ATL-PHYS-PUB-2013-009* (2013) .

[78] **CMS** Collaboration, A. M. Sirunyan *et al.*, "Identification of heavy-flavour jets with the CMS detector in pp collisions at 13 TeV," *JINST* **13** no. 05, (2018) P05011, arXiv:1712.07158 [physics.ins-det].

[79] G. Cowan, "Discovery sensitivity for a counting experiment with background uncertainty," *Technical report, Royal Holloway* (U.K) University of London.